The Radio Jets and Accretion Disk in NGC 4261

Dayton L. Jones

Jet Propulsion Laboratory, California Institute of Technology, Mail Code 238-332, 4800 Oak Grove Drive, Pasadena, CA 91109

Ann E. Wehrle

Infrared Processing and Analysis Center, Jet Propulsion Laboratory, California Institute of Technology, Mail Code 100-22, Pasadena, CA 91125

David L. Meier

Jet Propulsion Laboratory, California Institute of Technology, Mail Code 238-332, 4800 Oak Grove Drive, Pasadena, CA 91109

and

B. Glenn Piner

Jet Propulsion Laboratory, California Institute of Technology, Mail Code 238-332, 4800 Oak Grove Drive, Pasadena, CA 91109

ABSTRACT

The structure of AGN accretion disks on sub-parsec scales can be probed through free-free absorption of synchrotron emission from the base of symmetric radio jets. For objects in which both jet and counterjet are detectable with VLBI, the accretion disk will cover part of the counterjet and produce diminished brightness whose angular size and depth as a function of frequency can reveal the radial distribution of free electrons in the disk. The nearby (41 Mpc) FR-I radio galaxy NGC 4261 contains a pair of symmetric kpc-scale jets. On parsec scales, radio emission from the nucleus is strong enough for detailed imaging with VLBI. We present new VLBA observations of NGC 4261 at 22 and 43 GHz, which we combine with previous observations at 1.6 and 8.4 GHz to map absorption caused by an inner accretion disk. The relative closeness of NGC 4261 combined with the high angular resolution provided by the VLBA at 43 GHz gives us a very high linear resolution, approximately 2×10^{-2} pc $\approx$ 4000 AU $\approx$ 400 Schwarzchild radii for a 5×10^8 $M_\odot$ black hole.

The jets appear more symmetric at 1.6 GHz because of the low angular resolution available. The jets are also more symmetric at 22 and 43 GHz, presumably because the optical depth of free-free absorption is small at high frequencies. At 8.4 GHz neither confusion effect is dominant and absorption of counterjet emission by the presumed disk is detectable. We find that the orientation of the radio jet axis is the same on pc and kpc scales, indicating that the spin axis of the inner accretion disk and black hole has remained unchanged for at least 10^6 (and more likely $> 10^7$) years. This suggests that a single merger event may be responsible for the supply of gas in the nucleus of NGC 4261. The jet opening angle is between 0.3° and 20° during the first 0.2 pc of the jet, and must be $< 5°$ during the first 0.8 pc.

Assuming that the accretion disk is geometrically and optically thin and composed of a uniform 10^4 K plasma, the average electron density in the inner 0.1 pc of the disk is $10^3 - 10^8$ cm^{-3}. The mass of ionized gas in the inner pc of the disk is $10^1 - 10^3$ $M_\odot$, sufficient to power the radio source for $\sim 10^4 - 10^6$ years. Equating thermal gas pressure and magnetic field strength gives a disk magnetic field of $\sim 10^{-4} - 10^{-2}$ gauss at 0.1 pc. We include an appendix containing expressions for a simple, optically thin, gas pressure dominated accretion disk model which may be applicable to other galaxies in addition to NGC 4261.

Subject headings: accretion, accretion disks — galaxies: active — galaxies: individual (NGC 4261, 3C270) — galaxies: jets — galaxies: nuclei

1. Introduction

The structure of accretion disks in the inner parsecs of active galactic nuclei can be probed on sub-parsec scales through VLBI observations of free-free absorption of synchrotron radiation from the base of radio jets. The nearby radio galaxy NGC 4261 (3C270) contains a pair of highly symmetric kpc-scale jets (Birkinshaw and Davies 1985), and optical imaging with HST has revealed a large ($\sim$ 300 pc), nearly edge-on nuclear disk of gas and dust (Ferrarese, Ford, and Jaffe 1996). This suggests that the radio axis is close to the plane of the sky, consequently, relativistic beaming effects should be negligible. This orientation also precludes gravitational lensing by the central black hole from affecting the observed jet-to-counterjet brightness (Bao and Wiita 1997). In addition, the central milliarcsecond (mas) scale radio source is strong enough for imaging with VLBI (Jones, Sramek, and Terzian 1981). The combination of high angular resolution provided by VLBI at 43 GHz and the relative closeness of NGC 4261 (41 Mpc; Faber, et al. (1989)) give us a very high linear resolution, approximately 0.1 mas $\approx$ 0.02 pc $\approx$ 4000 AU $\approx$ 400 Schwarzchild radii for a 5×10^8 $M_\odot$ black hole. Thus, NGC 4261 is a good system both for the study of an edge-on accretion disk and for intrinsic differences between a jet and counterjet.

Our previous 8.4 GHz VLBA image of NGC 4261 (see Figure 4 in Jones and Wehrle (1997); hereafter JW) showed the inner parsec of the jet and counterjet, including a surprising narrow gap in emission at the base of the counterjet which we suspected was caused by free-free absorption in an accretion disk. The central brightness peak at 8.4 GHz was identified as the core by JW based on its inverted spectral index between 8.4 and 1.6 GHz. The gap seen at 8.4 GHz is similar to the even more dramatic gap seen in the center

of NGC 1052 (0238-084) at 15 GHz by Kellermann, et al. (1998). We report here 22 and 43 GHz VLBA observations which were made to map this gap with higher resolution. Our goals were to derive the physical characteristics of the disk, namely the allowed ranges of thickness, diameter, electron density, and magnetic field strength.

2. Observations

We observed NGC 4261 using 9 stations of the VLBA with full tracks on 7 September 1997, alternating 22-minute scans between 22.2 and 43.2 GHz. Good quality data were obtained from the Hancock, Fort Davis, Pie Town, Kitt Peak, Owens Valley, and Mauna Kea station, while rain affected North Liberty and Los Alamos and technical problems occurred at Brewster. The Saint Croix antenna was stowed due to hurricane Erika. Left circular polarization was recorded at both frequencies, with a total bandwidth of 64 MHz. Phase offsets between frequency channels were determined and corrected using both 3C273 and 1308+326.

The data were calibrated and fringe-fit using standard routines in AIPS[1] and imaging, deconvolution, and self-calibration were carried out in Difmap (Shepherd, Pearson, and Taylor 1994). Amplitude calibration of VLBI data at 22 and 43 GHz is often problematic due to rapidly changing tropospheric water vapor content. We checked our a priori amplitude calibration by comparing short-baseline flux densities of 3C273 with total flux density measurements made at 22 and 37 GHz with the 14-m Metsäehovi antenna. In both cases our flux densities agree with those from Metsaehovi to within 15%.

An 8.4 GHz image of NGC 4261, made in a similar manner from VLBA data obtained

[1]The Astronomical Image Processing System was developed by the National Radio Astronomy Observatory.

in April 1995, is shown in Figure 1 for comparison with our newer, higher frequency images. The beam size at 8.4 GHz was 1.84×0.80 mas with the major axis almost exactly north-south. Figure 2 illustrates a possible geometry of the central region which is consistent with the radio morphology seen in Figure 1.

EDITOR: PLACE FIGURE 1 HERE.

EDITOR: PLACE FIGURE 2 HERE.

The full resolution (uniform weighting, no taper) VLBA images at 22 and 43 GHz are shown in Figures 3 and 4, respectively. The beam sizes at 22 and 43 GHz are 1.06×0.29 mas and 0.61×0.16 mas, with the major axis within 20° of north-south. We also made naturally weighted images at both frequencies to search for more extended emission, but no detectable emission was found outside of the area shown in Figures 3 and 4.

EDITOR: PLACE FIGURE 3 HERE.

EDITOR: PLACE FIGURE 4 HERE.

In addition, Figure 5 shows the 43 GHz image after convolution with the same restoring beam as used in Figure 3 to allow spectral index measurements. The same field of view is shown in Figures 3 and 5.

EDITOR: PLACE FIGURE 5 HERE.

The wide range of baseline lengths provided by the VLBA makes it possible to obtain sufficient overlap of the (u,v) coverage between 22 and 43 GHz for spectral index determinations. However, the correct offset between our 22 and 43 GHz images is not known a priori because we do not have absolute positions. A range of plausible offsets was tried, with the most likely result being a shift of the 22 GHz image 0.125 mas west with respect to the 43 GHz image. This offset is less than half of the E-W beam width in figures 3 and 5, and minimizes the total range of spectral index values. The spectral index map made with this offset is shown in figure 6. Note that relatively small changes in offset can produce large changes in the spectral index map, so the spectral index distribution in figure 6 is plausible but not definitive.

EDITOR: PLACE FIGURE 6 HERE.

To see if amplitude self-calibration had significantly changed the flux density scales of our 22 or 43 GHz images, we compared the peak surface brightness from images made with only phase self-calibration and images made with full amplitude and phase self-calibration. The resulting amplitude corrections applied to the data were 19% at 22 GHz and 12% at 43 GHz. Uncertainties in the absolute flux density scales can shift all of the spectral index valuse in figure 6 by a constant amount, but will not change the shape of the distribution. Note that the most inverted spectral slope occurs at the position of the presumed accretion disk absorption and not at the position of the bright compact core. The spectrum becomes steeper away from the central core and accretion disk region.

3. Results

3.1. The Parsec-scale Radio Jets

The position angle of the jets is $87° \pm 8°$ in our VLBI images, and $88° \pm 2°$ on VLA images (Birkinshaw and Davies 1985). The orientation of the jet axis remains the same on kpc and sub-pc scales, indicating that the spin axis of the inner accretion disk and black hole has remained unchanged for at least 10^6 years (assuming an average expansion speed of 0.1 c), and possibly much longer.

A comparison of our 8, 22, and 43 GHz VLBA images indicates that the region just east of the core, including the first half parsec of the counterjet, has a highly inverted spectrum ($\alpha > 0$, where $S_\nu \propto \nu^\alpha$). It is plausible that free-free absorption by gas in the central accretion disk is responsible for this. The jet and counterjet both have steep radio spectra ($\alpha < 0$) far from the core, as expected. Note that if the free-free absorption model is correct, the most inverted spectrum may not be located at the position of the true core (the "central engine").

We can set an upper limit for the jet opening angle by noting that the jet appears unresolved in the transverse (north-south) direction out to at least 4 mas from the absorption feature in Figure 1. Using one quarter of the N-S beam width as an upper limit to the extent of emission in the transverse jet direction gives an upper limit of 5° for the full opening angle during the first 0.8 pc of the jet. A lower limit for the opening angle can be obtained by requiring that the angular size of emission at the location of the bright peak 1 mas from the absorption feature in Figure 1 be large enough to avoid synchrotron self-absorption. This requires an opening angle of $> 0.3°$ during the first 0.2 pc of the jet. Since we believe that the radio jets in NGC 4261 are nearly perpendicular to our line of sight, projection effects should be minimal and the intrinsic jet opening angle θ is

$0.3° < \theta < 20°$ during the first 0.2 pc of the jet and $\theta < 5°$ during the first 0.8 pc of the jet.

Since emission from both the jet and counterjet is detectable with VLBI, it may be possible to measure proper motions on both sides of the core in this source. If so, the orientation of the radio jets with respect to our line of sight can be found, and any resulting small relativistic beaming effects on the jet/counterjet brightness can be taken into account. A more sensitive 43 GHz VLBI image (where free-free absorption is minimal) can then be used to see just how similar the jet acceleration and collimation processes are on both sides of a "central engine" at the same epoch.

3.2. The Inner Accretion Disk

The fact that our 1.6 GHz image (see Figure 1 in JW) is highly symmetric lets us set an upper limit to the angular size of any absorption feature. At this frequency the free-free optical depth should be large, so to avoid detection the angular size of the absorption feature must be much smaller than our angular resolution at 1.6 GHz. The restoring beam in Figure 1 of JW has an east-west size of 9 mas. The jet/counterjet brightness ratio is unity from the core out to at least ±25 mas. Using the observed brightness ratio of ≈ 1 at ±10 mas ($\sim \pm 2$ pc), just larger than our resolution, tells us that the transverse size of any deep absorption feature is $<<$ 2 pc. It is expected that the inner pc or so of an accretion disk orbiting a massive ($\sim 10^8 - 10^9$ $M_\odot$) black hole will be geometrically thin, and consequently we will assume a typical disk thickness of $<<$ 0.1 pc and a nominal line-of-sight path length through the inner disk of $\sim$ 0.1 pc. We now use the HI and CO column densities measured by Jaffe and McNamara (1994), $\approx 10^{21}$ cm^{-2}, to estimate an electron number density of $n_e \geq 3 \times 10^3\ (0.1/L)$ cm^{-3}, where L is the path length in pc. A slightly lower density would be deduced using the X-ray absorption column density of $N_H < 4 \times 10^{20}$ cm^{-2} from Worrall and Birkinshaw (1994). In both cases it is assumed that there will be on average one free

electron per nucleus. This is a conservative assumption since the inner 0.1 pc of the disk should be highly ionized and have a density at least as large as the outer neutral regions. The inclination of the disk is needed to further constrain the path length L and thus the average electron density n_e.

To get an upper limit for n_e, we note that the jet/counterjet brightness ratio at 43 GHz near the core in Figure 5 is also small (≈ 2). This implies a low optical depth at 43 GHz. Assuming an electron temperature of $\sim 10^4$ K (plausible at a disk radius of 0.1 pc), an optical depth $\tau < 1$ at 43 GHz requires $n_e < 4 \times 10^5 \sqrt{0.1/L}$ cm^{-3}. However, the temperature of the disk increases at smaller radii, possibly reaching $10^7 - 10^8$ K near the inner edge. At these temperatures, an electron number density of $\sim 10^8 \sqrt{0.1/L}$ cm^{-3} is needed to produce an optical depth of unity at 43 GHz. The upper limit for electron number density will be somewhere between $4 \times 10^5 \sqrt{0.1/L}$ and $10^8 \sqrt{0.1/L}$ cm^{-3}, depending on the actual range of electron temperatures along the line of sight.

Thus, the electron number density of the inner accretion disk, averaged over the line of sight, is

$$3 \times 10^3 \, (0.1/L) \; < \; n_e \; < \; 10^8 \sqrt{0.1/L} \;\; \mathrm{cm}^{-3}.$$

For comparison, the inner accretion disk believed to be responsible for the unusually inverted spectrum of the radio core in Centaurus A has an average electron number density of at least 10^5 cm^{-3} for a path length of 1 pc (Jones, et al. 1996). Assuming a thin inner disk in NGC 4261 with a radius of 1 pc and a thickness of 0.01 pc, an average electron density of 10^6 cm^{-3}, and one proton per electron, the mass of ionized gas in the disk is $\sim 10^3$ M$_\odot$. Of course, a larger assumed thickness or radius would lead to a larger inner accretion disk mass. Even 10^3 M$_\odot$ is sufficient to fuel the central engine for 10^6 years at an accretion rate of 10^{-3} M$_\odot$ per year, consistent with the observed luminosity. A more realistic disk model with thickness increasing with radius and density decreasing with radius

is described in Appendix A. This model predicts a lower total mass of ionized gas within 1 pc, which implies that material must migrate through the disk from radii > 1 pc during the source lifetime. It is interesting to note that the electron number density we derive at 0.1 pc is comparable to that in the solar corona at ~ 2 $R_\odot$.

Equating the thermal gas pressure in the disk with the local magnetic field ($B^2 = 8\pi\ \alpha\ n_e kT$, where $\alpha \approx 0.01$ is the usual viscosity parameter; Shakura and Sunyaev (1973)) gives a disk magnetic field of $\sim 10^{-2} - 10^{-4}$ gauss at 0.1 pc. General expressions for estimating physical parameters in an optically thin, gas pressure dominated accretion disk at radii of $\sim 0.1 - 1$ pc are derived in Appendix A. Table 1 compares these parameter values with those for other galaxies in which there is evidence for an inner accretion disk. Of the five nearby (< 100 Mpc) radio galaxies for which some inner accretion disk characteristics are known, only two (NGC 4261 and NGC 4258) have well-determined central black hole masses (see Table 1).

4. Discussion

A geometrically thin inner disk which would not completely obscure optical emission from the core is a plausible model given the very high percentage of low luminosity 3CR radio galaxies which have bright, unresolved optical continuum sources visible on HST/WFPC2 images (Chiaberg, Capetti, and Celotti 1998). This includes NGC 4261. A geometrically and optically thick dusty torus would obscure the central optical continuum source in many low luminosity objects with FR I radio morphology, since these sources are expected to be oriented at large angles to our line of sight. A nearly edge-on disk orientation may also explain the low bolometric luminosity of the NGC 4261 nucleus and lack of an ultraviolet excess in its spectral energy distribution (Ho 1999). Additional constraints on the inclination and density of the inner disk could come from observations of free-free

radio emission from ionized disk gas or radio emission from the central jets scattered by electrons in the far inner edge of the accretion disk (Gallimore, Baum, and O'Dea 1997). However, the dynamic range of our VLBA images is not adequate to detect this emission in the presence of the bright parsec-scale radio jets. Another way to constrain the radio axis, and thus the inner disk, orientation would be measurement of proper motions in both the jet and counterjet (e.g., Taylor, Wrobel, and Vermeulen (1998)). VLBA observations to attempt this are underway.

The above analysis makes use of the fact that the observed jet/counterjet brightness ratio in NGC 4261, and in some other galaxies which are well-observed with VLBI, peaks at intermediate frequencies and falls to nearly unity at both low frequencies (where the beam is much larger than the angular size of the absorbing material) and high frequencies (where the free-free optical depth becomes very small). See, for example, Figure 15 in Krichbaum, et al. (1998). At low frequencies the brightness ratio R should decrease approximately linearly with frequency ($\theta_{\rm beam} \propto \nu^{-1}$), while at high frequencies the fall-off of R should be more rapid ($\tau_{\rm f-f} \propto \nu^{-2}$). With VLBA images at four frequencies we can not confirm this behaviour in detail, but it is clear that near the core the brightness ratio R is greater at 8.4 GHz than at 1.6, 22, or 43 GHz.

The mass of the central black hole in NGC 4261 is $(5 \pm 1) \times 10^8$ $M_\odot$ (Ferrarese, Ford, and Jaffe 1996). Thus, the mass of material in the inner accretion disk is negligible compared to the black hole mass, and the orbital period of material in the inner accretion disk at a radius r (in pc) is $\approx 4 \times 10^9$ $(r/0.1)^{3/2}$ seconds ($\approx 10^2$ years for $r = 0.1$ pc). The spin rate of the central black hole is unknown, but is predicted to be small by the model of Meier (1999). A lower limit on the spin of the black hole can be derived from the known mass of the hole, the assumed accretion rate (10^{-3} $M_\odot$ per year), and the spin axis alignment timescale ($> 10^6$ years) implied by the co-linear kpc scale jets. The resulting

dimensionless spin parameter (see Misner, Thorne, and Wheeler (1973)) is $> 2 \times 10^{-4}$, which allows either high or low black hole spin rates.

The angular momentum of gas in the inner accretion disk is expected to be aligned with the spin axis of the black hole (Bardeen and Petterson 1975). If the black hole is spinning slowly, its spin axis will eventually become aligned with the angular momentum of the accreting gas at large radii (Natarajan and Pringle 1998). However, the long-term directional stability of the radio jets in NGC 4261 implies that the gas falling into the central region of the galaxy and supplying the central engine has had a constant angular momentum direction for most of the life of the radio source. This in turn implies that a single merger event may be responsible for the supply of gas in the nucleus of NGC 4261.

5. Conclusions

We have imaged the nuclear radio source in NGC 4261 with the VLBA at four frequencies. We find that the jet/counterjet brightness ratio near the core is larger at 8.4 GHz than at lower frequencies. This can be explained by a combination of two effects: low angular resolution at 1.6 GHz which masks small-scale brightness variations, and low absorption by ionized thermal gas at 22 and 43 GHz. The brightness asymmetry at 8.4 GHz could be caused by a nearly edge-on inner accretion disk. If so, the (model dependent) electron density in the inner 0.1 pc of the disk has an average value between 3×10^3 and 10^8 cm^{-3}. Future observations to measure proper motions in the jet and counterjet will better define the orientation of the radio axis and thus the inclination of the inner accretion disk. This will determine the path length L through the disk, and consequently reduce the allowable range of electron number density averaged over the path length.

The optically thin, uniform temperature model disk described in the appendix, derived

only from accretion physics and values of the black hole mass and accretion rate consistent with NGC 4261, is remarkably similar to the disk that we observe in free-free absorption against the radio jet. We therefore believe that these observations have detected the sub-pc accretion disk powering the active nucleus in NGC 4261.

The Very Long Baseline Array is part of the National Radio Astronomy Observatory, which is a facility of the National Science Foundation operated by Associated Universities, Inc., under a cooperative agreement with the NSF. A.W. gratefully acknowledges support from the NASA Long Term Space Astrophysics Program. We thank H. Teräsranta for making the Metsäehovi flux density measurements of 3C273 available. This research was carried out at the Jet Propulsion Laboratory, California Institute of Technology, under contract with the National Aeronautics and Space Administration.

A. Isothermal, Optically-thin Accretion Disks far from Black Holes

In this appendix we describe a simple accretion disk model, suitable for optically thin gas-pressure dominated flow far from the black hole, in which the plasma temperature is a very slowly varying function of distance from the hole. The canonical temperature is assumed to be 10^4K for the range of interest in this model. (Such a temperature is typical of an optically thin, warm plasma undergoing moderate heating to keep it mostly ionized.) Following Shakura and Sunyaev (1973), and ignoring the factor of $(1 - r^{-1/2}) \approx 1$ (since at $0.1 - 1.0$ pc, $r = R/3R_{Sch} = 3400 - 34,000$ for a $10^8 M_\odot$ black hole), we obtain the following equations for the disk structure, expressed in units of $M_8 \equiv M_{BH}/10^8 M_\odot$ for the black hole mass, $\dot{M}_{-3} \equiv \dot{M}/(10^{-3} M_\odot \, \mathrm{yr}^{-1}) = \dot{M}/(6.3 \times 10^{22} \mathrm{g\,s}^{-1})$ for the accretion rate, and $R_{18} \equiv R/10^{18}$cm for the distance from the black hole.

From the equation for hydrostatic equilibrium in the direction perpendicular to the

disk, the disk half-thickness is

$$H \;=\; 0.0026\,\mathrm{pc}\; M_8^{-1/2}\; R_{18}^{3/2} \tag{A1}$$

For NGC 4261, with $M_8 = 5$, the *full* disk thickness at a radius of 1 pc ($R_{18} = 3$) is 0.012 pc, very close to the 0.01 pc thickness assumed for the simple uniform thickness disk in section 3.2. Adopting a radiative cooling rate of $\sim 3 \times 10^{-23}\; n^2$ erg cm^{-3} at 10^4K (Krolik 1999) and setting it equal to the energy generated locally by viscous (accretion) heating, we obtain the particle density

$$n \;=\; 1.5 \times 10^4\,\mathrm{cm}^{-3}\; M_8^{3/4}\; \dot{M}_{-3}^{1/2}\; R_{18}^{-9/4} \tag{A2}$$

The approximate optical depth of the disk in a direction perpendicular to it, due to the inverse absorption processes (at $\nu \sim kT/h \approx$ optical frequencies), is

$$\tau_{abs} \;=\; 1.4 \times 10^{-11}\; M_8\; \dot{M}_{-3}\; R_{18}^{-3} \tag{A3}$$

and that due to electron scattering is

$$\tau_{es} \;\leq\; 1.5 \times 10^{-4}\; M_8^{1/4}\; \dot{M}_{-3}^{1/2}\; R_{18}^{-3/4} \tag{A4}$$

(an upper limit, since the gas is not fully ionized). At IR-optical-UV wavelengths, therefore, the disk is very optically thin. It becomes optically thick to free-free absorption in the perpendicular direction ($\kappa_\nu\, m_p\, n\, 2H \geq 1$) only below the frequency

$$\nu_{perp} \;=\; 250\,\mathrm{MHz}\; M_8^{1/2}\; \dot{M}_{-3}^{1/2}\; R_{18}^{-3/2} \tag{A5}$$

However, if viewed nearly edge-on, with the line-of-sight passing roughly from $R_{18}/3$ to $3R_{18}$ (*i.e.*, $0.1 - 1.0$ pc), the disk will be optically thick to free-free ($\int \kappa_\nu\, m_p\, n\, dR \geq 1$) below the frequency

$$\nu_{edge-on} \;=\; 8\,\mathrm{GHz}\; M_8^{3/4}\; \dot{M}_{-3}^{1/2}\; R_{18}^{-7/4} \tag{A6}$$

For $M_8 = 5$ we get

$$\nu_{edge-on} = 27\,\mathrm{GHz}\ \dot{M}_{-3}^{1/2}\ R_{18}^{-7/4} \tag{A7}$$

The mass of the disk within this radius range, and flow time scale (R/v_R), are

$$M_{disk} = 3.9\,\mathrm{M}_\odot\ M_8^{1/4}\ \dot{M}_{-3}^{1/2}\ R_{18}^{5/4} \tag{A8}$$

$$t_{acc} = 1200\,\mathrm{yr}\ M_8^{1/4}\ \dot{M}_{-3}^{-1/2}\ R_{18}^{5/4} \tag{A9}$$

Three consistency checks on the model are the ratio of the half-thickness to disk radius at a given point, the ratio of the accretion (inflow) velocity to the Keplerian velocity, and the ratio of inward heat advection to radiative cooling, all of which should be small, given the assumptions of the model. We find that

$$\frac{H}{R} = 0.008\ M_8^{-1/2}\ R_{18}^{1/2} \tag{A10}$$

for the disk height,

$$\frac{-v_R}{v_K} = 0.23\ M_8^{-3/4}\ \dot{M}_{-3}^{1/2}\ R_{18}^{1/4} \tag{A11}$$

for the inflow velocity, and

$$\frac{\dot{\varepsilon}_{adv}}{\dot{\varepsilon}_{rad}} = 2.5 \times 10^{-4}\ M_8^{-1}\ R_{18} \tag{A12}$$

for the magnitude of the advection of thermal energy. Each of these three ratios will be even smaller if $M_8 = 5$, the value appropriate for NGC 4261, is used. (Note that, because of the low optical depth, the photon distribution is not a black body and has an even lower energy density than the thermal gas.) The assumption of a thin, radiating, 10^4K, Keplerian accretion disk, therefore, is consistent with the model calculations, as well as with our observational results for the absorbing disk in NGC 4261.

REFERENCES

Bao, G., and Wiita, P. J. 1997, ApJ, 485, 136

Bardeen, J. M., and Petterson, J. A. 1975, ApJ, 195, L65

Birkinshaw, M., and Davies, R. L. 1985, ApJ, 291, 32

Braatz, J. A., Claussen, M. J., Diamond, P. J., Wilson, A. S., and Henkel, C. 1999, BAAS, 31, 899 (paper 50.19, June 1999 AAS meeting)

Chiaberge, M., Capetti, A., and Celotti, A. 1998, 19th Texas Symposium on Rel. Astrophys. & Cosmology (Paris), poster.

Dhawan, V., Kellermann, K. I., and Romney, J. D. 1998, ApJ, 498, L111

Faber, S. M., Wegner, G., Burstein, D., Davies, R. L., Dressler, A., Lynden-Bell, D., and Terlevich, R. J. 1989, ApJS, 69, 763

Ferrarese, L., Ford, H. C., and Jaffe, W. 1996, ApJ, 470, 444

Gallimore, J. F., Baum, S. A., and O'Dea, C. P. 1997, Nature, 388, 852

Herrnstein, J. R. et al. 1997, ApJ, 475, L17

Herrnstein, J. R. et al. 1998, ApJ, 508, 243

Ho, L. C. 1999, ApJ, 516, 672

Jaffe, W., and McNamara, B. R. 1994, ApJ, 434, 110

Jones, D. L., Sramek, R. A., and Terzian, Y. 1981, ApJ, 246, 28

Jones, D. L., et al. 1996, ApJ, 466, L63

Jones, D. L., and Wehrle, A. E. 1997, ApJ, 484, 186

Kellermann, K. I., Vermeulen, R. C., Zensus, J. A., and Cohen, M. H. 1998, AJ, 115, 1295

Kellermann, K. I., Vermeulen, R. C., Cohen, M. H., and Zensus, J. A. 1999, BAAS, 31, 856 (paper 20.02, June 1999 AAS meeting)

Krichbaum, T. P., Alef, W., Witzel, A., Zensus, J. A., Booth, R. S., Greve, A., and Rogers, A. E. E. 1998, A&A, 329, 873

Krolik, J. H. 1999, Active Galactic Nuclei, (Princeton, NJ: Princeton Univ. Press)

Meier, D. L. 1999, ApJ, 522, 753

Misner, C. W., Thorne, K. S., and Wheeler, J. A. 1973, Gravitation (San Francisco: Freeman)

Natarajan, P., and Pringle, J. E. 1998, ApJ, 506, L97

Peck, A. B., Taylor, G. B., and Conway, J. E. 1999, ApJ, 521, 103

Shakura, N. I., and Sunyaev, R. A. 1973, A&A, 24, 337

Shepherd, M. C., Pearson, T. J., and Taylor, G. B. 1994, BAAS, 26, 987

Taylor, G. B., Wrobel, J. M., and Vermeulen, R. C. 1998, ApJ, 498, 619

Tingay, S. J., et al. 1998, AJ, 115, 960

Ulvestad, J. S., Wrobel, J. M., Roy, A. L., Wilson, A. S., Falcke, H., and Krichbaum, T. P. 1999, ApJ, 517, 81

Worrall, D. M., and Birkinshaw, M. 1994, ApJ, 427, 134

This manuscript was prepared with the AAS LaTeX macros v5.0.

Fig. 1.— VLBA image of NGC 4261 at 8.387 GHz. The contour levels are 1, 2, 4, 8, 16, 32, and 64% of the peak surface brightness (101 mJy/beam). The restoring beam is 1.84×0.80 mas with the major axis along position angle -1.1°.

Fig. 2.— Schematic illustration of the central few parsecs in NGC 4261 showing the relative positions of the core (black hole), jet, counterjet, and inner accretion disk.

Fig. 3.— Full resolution 22-GHz VLBA image, showing the first parsec of the radio jet and counterjet as well as the bright, barely resolved core. The jet-to-counterjet brightness ratio at ± 1 mas from the core is significantly smaller at 22 GHz than at 8.4 GHz (see Figures 3 and 4 in JW). The contours are -1, 1, 2, 4, 8, 16, 32, and 64% of the peak (165 mJy/beam), and the restoring beam is 1.06×0.29 mas with the major axis along position angle -18.3°. The total flux density in the image is 388 mJy.

Fig. 4.— Full resolution 43-GHz VLBA image. The contours are -1, 1, 2, 4, 8, 16, 32, and 64% of the peak (141 mJy/beam), and the restoring beam is 0.61×0.16 mas with the major axis in position angle -19.5°. Figures 1 and 4 have the same field of view. The total flux density in the image is 478 mJy.

Fig. 5.— 43-GHz image convolved with the same restoring beam as the 22-GHz image in Figure 3 to allow spectral indices to be measured. The contours levels are 1, 2, 4, 8, 16, 32, and 64% of the peak (305 mJy/beam) with the major axis along position angle -18.3°. Residuals have not been included in this image. Note that Figures 3 and 5 cover the same field of view. Although only the innermost parts of the jet and counterjet are detectable at

43 GHz, the brightness ratio near the core is closer to unity than it is at lower frequencies.

Fig. 6.— 22-43 GHz spectral index map made by combining figures 3 and 5 with an E-W offset of 0.125 mas (22 GHz peak west of 43 GHz peak). The image has been clipped at three times the rms noise level. The gray scale gives the value of the spectral index α from -1.8 (steep) to +2.2 (inverted). Scale errors will shift all spectral index values in the figure by a constant amount, but will not change the shape of the distribution.

Table 1: Characteristics of Accretion Disks

Source name	Dist. Mpc[†]	$S_{\rm jet}$ (Jy)[‡]	Height (pc)	Radius (pc)	n_e (cm^{-3})	Disk mag. field (G)	M_{BH} ($M_\odot$)	Assumed tmp. (K)	Ref.
NGC 5128	3.5	7.0	< 1	> 1	$> 10^5$	$> 2 \times 10^{-3}$	–	10^4	1
NGC 4258	6.4	0.003	< 0.1	~ 0.3	–	$\leq 3 \times 10^{-1}$	3.5×10^7	N/A	2
NGC 1052	17	1.0	~ 0.1	> 1	$\sim 10^5$	3×10^{-3}	–	10^4	3
NGC 4261	41	0.5	~ 0.01	~ 0.1	$\sim 10^6$	$10^{-4} - 10^{-2}$	5×10^8	10^4	4
Mkn 348	56	0.5 v	~ 0.1	~ 1	$10^5 - 10^7$	$\approx 6 \times 10^{-4}$	–	8×10^3	5
Mkn 231	168	0.03 v	~ 0.1	~ 1	$10^5 - 10^7$	$\approx 6 \times 10^{-4}$	–	8×10^3	5
Cygnus A	225	1. v	< 0.3	< 15	$> 7 \times 10^3$	$> 4 \times 10^{-4}$	–	$> 3 \times 10^3$	6
1946+708	400	0.3	< 20	< 50	$> 2 \times 10^2$	$> 10^{-5}$	–	8×10^3	7
NGC 1275	700	30. v	~ 0.1	> 25.0	$\sim 7 \times 10^4$	8×10^{-4}	$\sim 10^8$	10^4	8

[†] Using $H_0 = 75$ km s^{-1} Mpc^{-1} for distances given as redshifts

[‡] "v" indicates variability

Table 1 references:

1. Jones, et al. 1996; Tingay, et al. 1998.
2. Herrnstein, et al. 1997; 1998.
3. Braatz, et al. 1999; Kellermann, et al. 1999.
4. This paper.
5. Ulvestad, et al., 1999.
6. Krichbaum, et al. 1998.
7. Peck, et al. 1999.
8. Dhawan, et al. 1998.

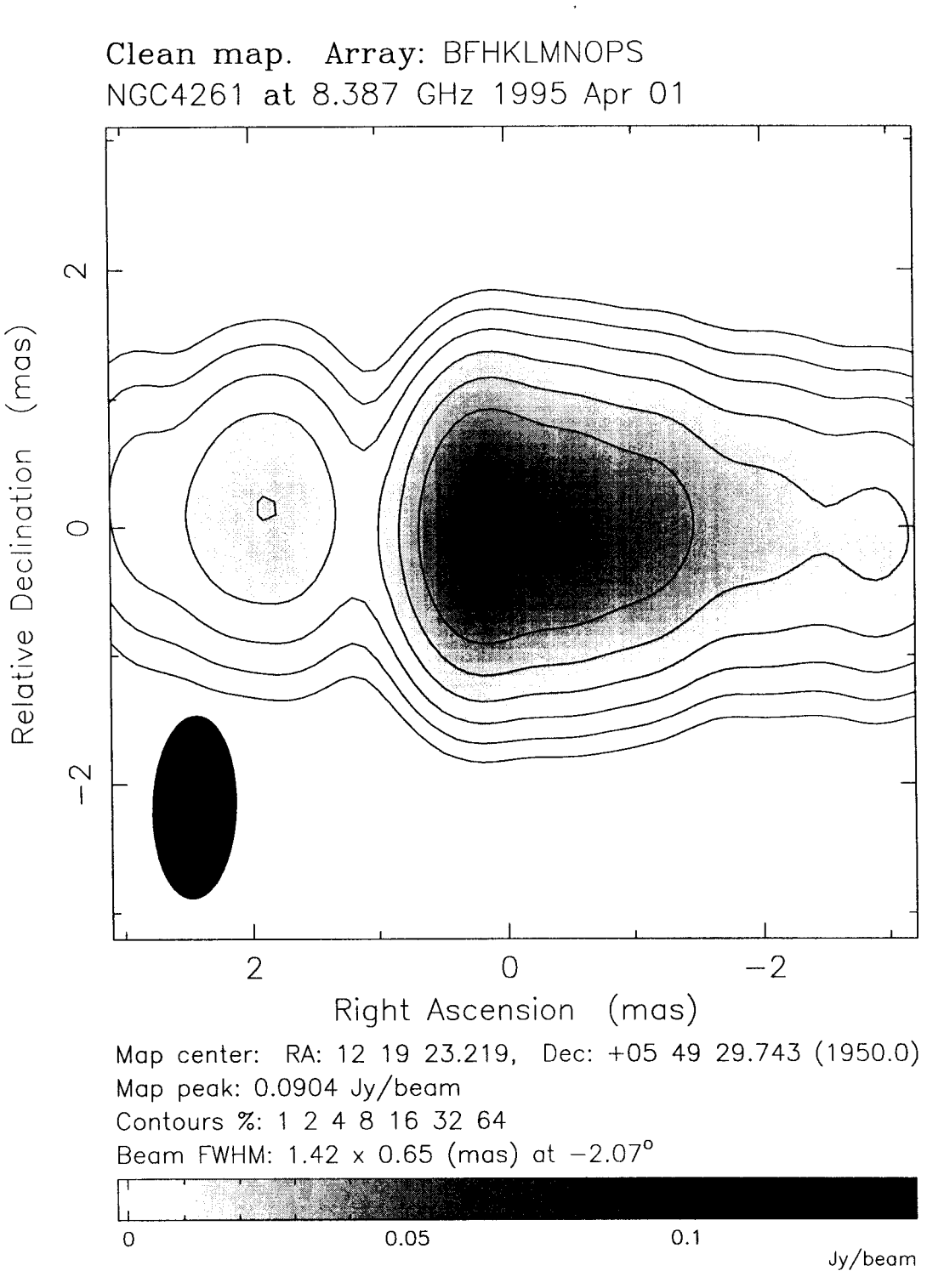
Clean map. Array: BFHKLMNOPS
NGC4261 at 8.387 GHz 1995 Apr 01
Relative Declination (mas)
2
0
−2
2
0
−2
Right Ascension (mas)
Map center: RA: 12 19 23.219, Dec: +05 49 29.743 (1950.0)
Map peak: 0.0904 Jy/beam
Contours %: 1 2 4 8 16 32 64
Beam FWHM: 1.42 x 0.65 (mas) at −2.07°
0
0.05
0.1
Jy/beam

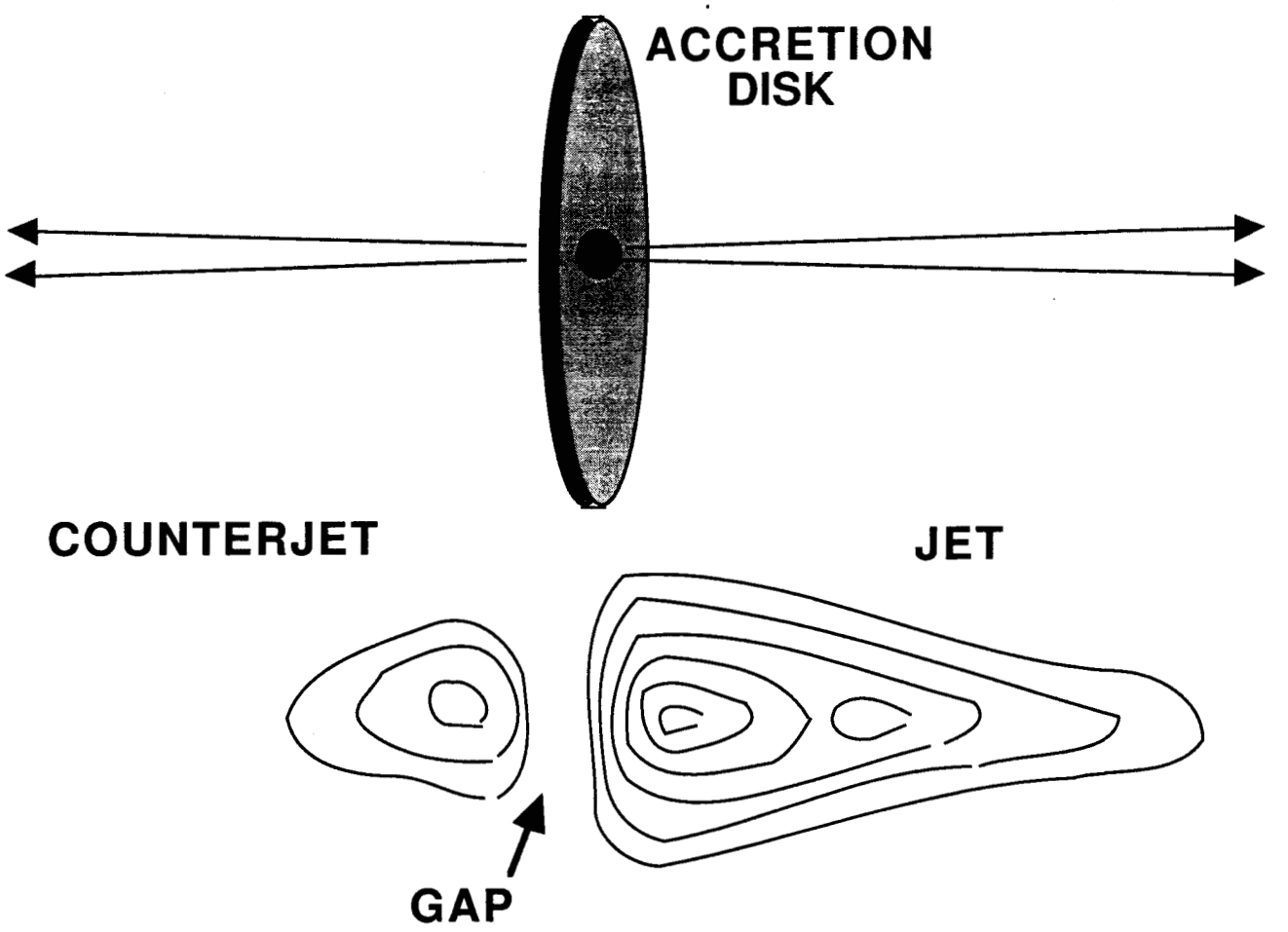
ACCRETION
DISK
COUNTERJET
JET
GAP

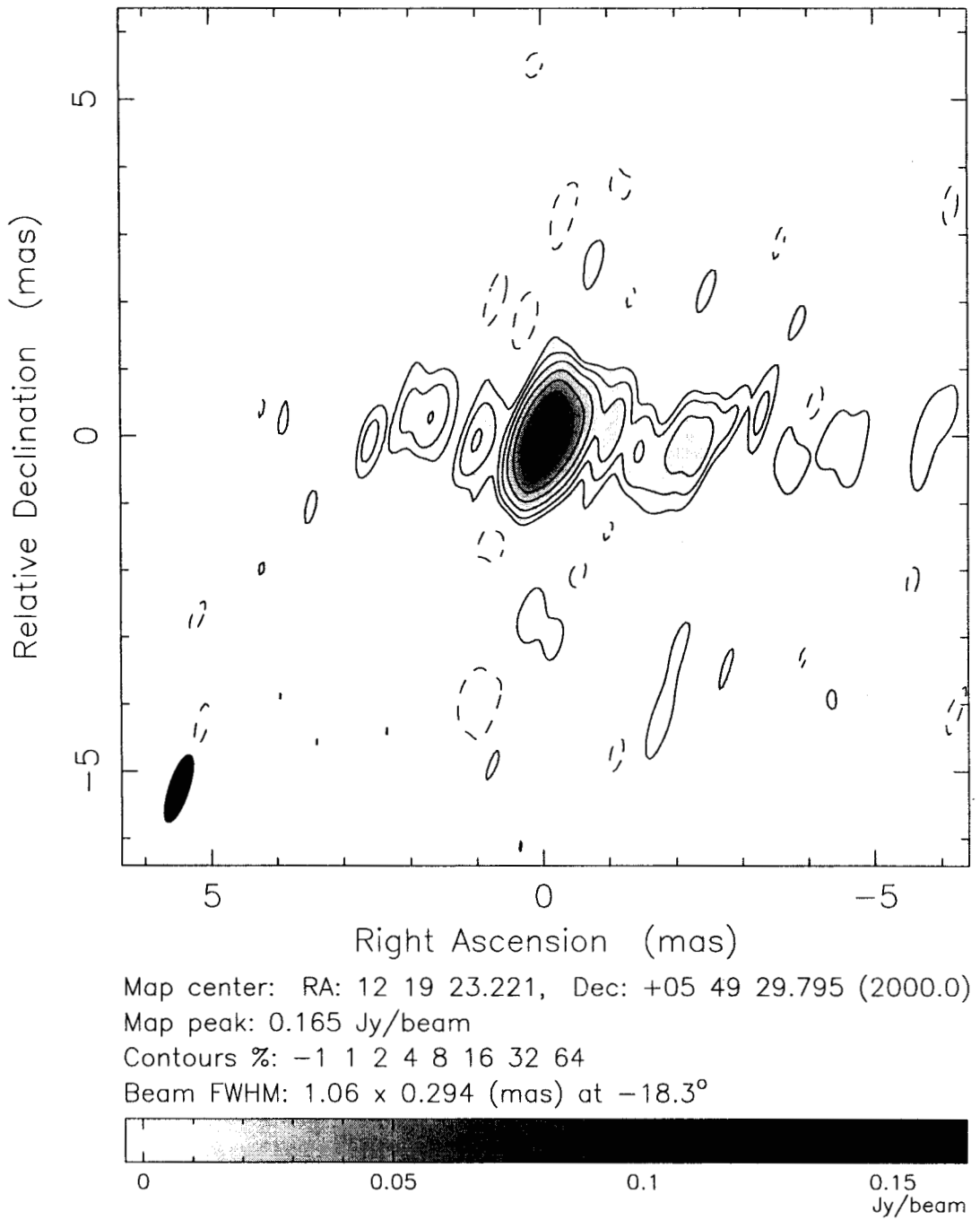
Clean map. Array: BFHKLMNOP
NGC4261 at 22.206 GHz 1997 Sep 07
Relative Declination (mas)
5
0
−5
5
0
−5
Right Ascension (mas)
Map center: RA: 12 19 23.221, Dec: +05 49 29.795 (2000.0)
Map peak: 0.165 Jy/beam
Contours %: −1 1 2 4 8 16 32 64
Beam FWHM: 1.06 x 0.294 (mas) at −18.3°
0
0.05
0.1
0.15
Jy/beam

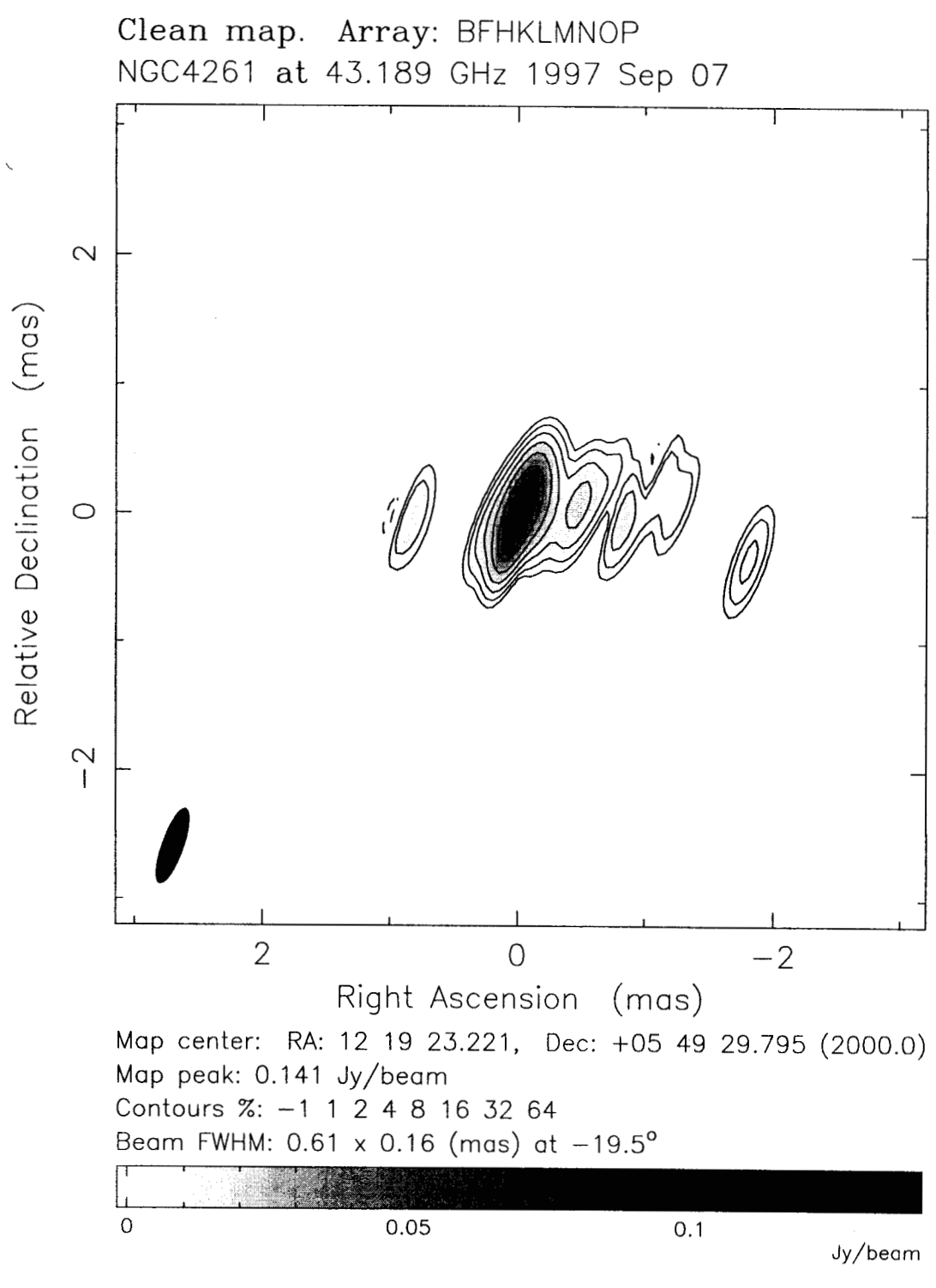
Clean map. Array: BFHKLMNOP
NGC4261 at 43.189 GHz 1997 Sep 07
Relative Declination (mas)
2
0
−2
2
0
−2
Right Ascension (mas)
Map center: RA: 12 19 23.221, Dec: +05 49 29.795 (2000.0)
Map peak: 0.141 Jy/beam
Contours %: −1 1 2 4 8 16 32 64
Beam FWHM: 0.61 x 0.16 (mas) at −19.5°
0
0.05
0.1
Jy/beam

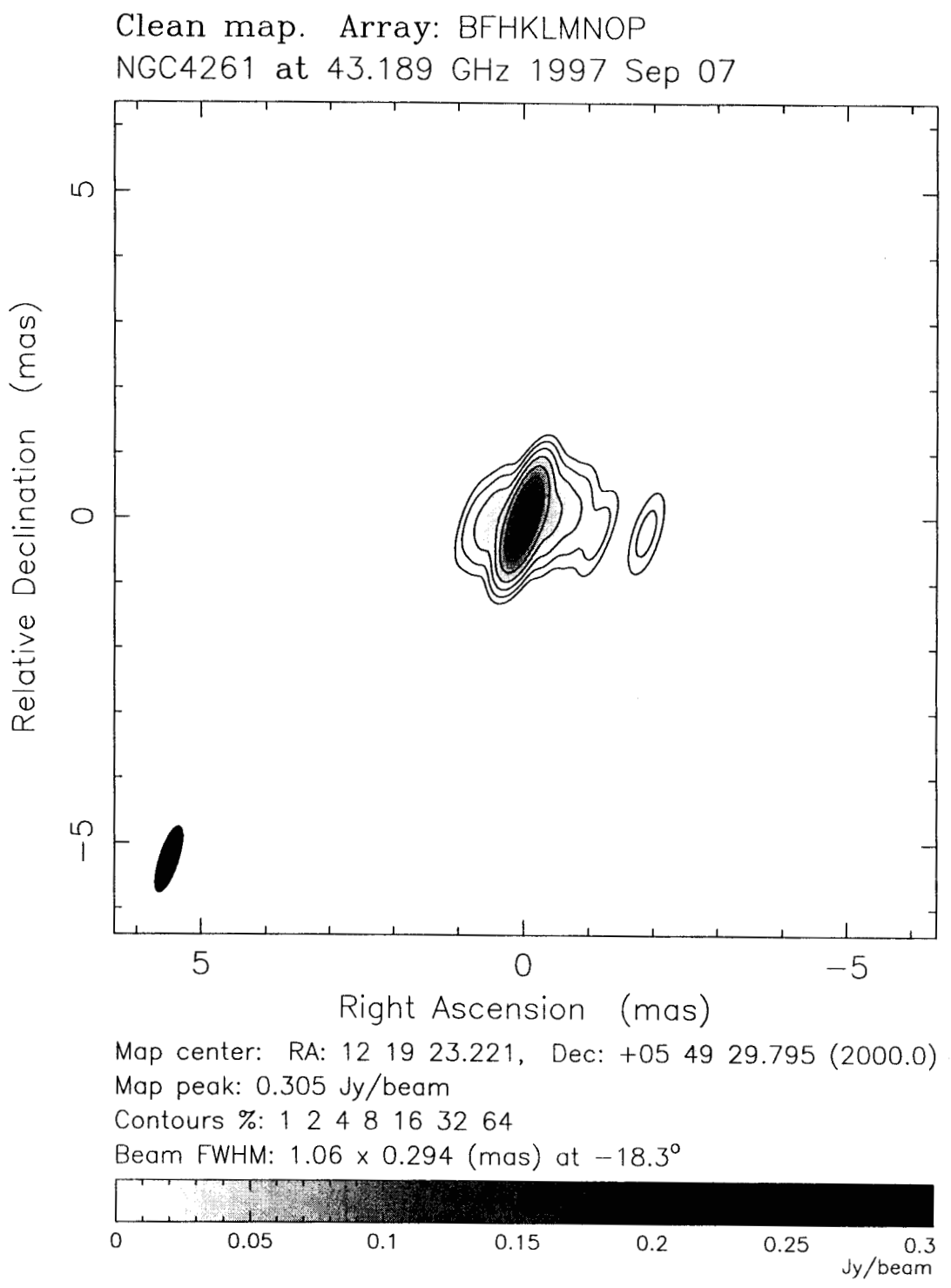
Clean map. Array: BFHKLMNOP
NGC4261 at 43.189 GHz 1997 Sep 07
Relative Declination (mas)
5
0
−5
5
0
−5
Right Ascension (mas)
Map center: RA: 12 19 23.221, Dec: +05 49 29.795 (2000.0)
Map peak: 0.305 Jy/beam
Contours %: 1 2 4 8 16 32 64
Beam FWHM: 1.06 x 0.294 (mas) at −18.3°
0
0.05
0.1
0.15
0.2
0.25
0.3
Jy/beam

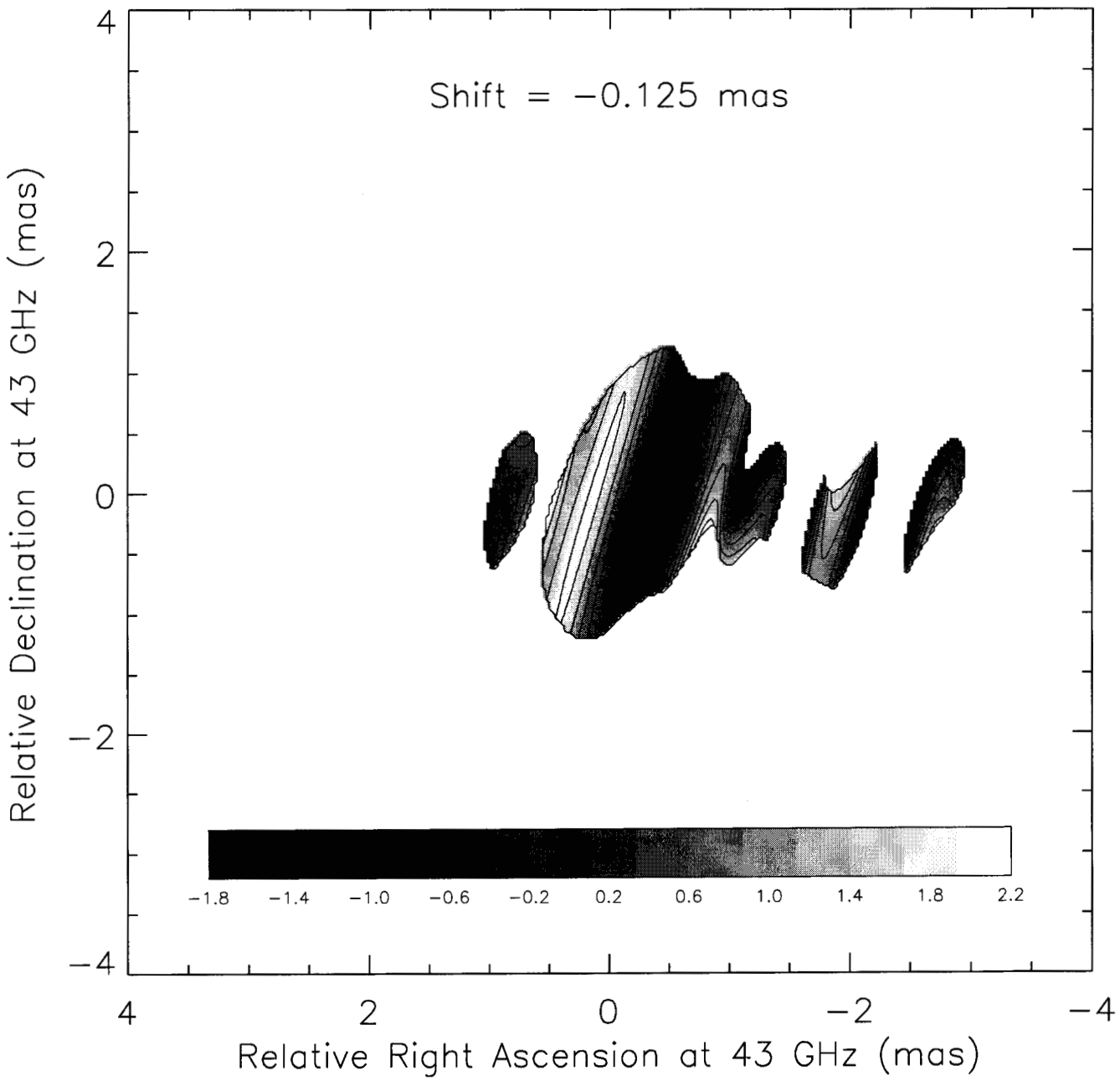
Shift = −0.125 mas
Relative Declination at 43 GHz (mas)
Relative Right Ascension at 43 GHz (mas)
4
2
0
−2
−4
−1.8
−1.4
−1.0
−0.6
−0.2
0.2
0.6
1.0
1.4
1.8
2.2